Molecular Dynamics Simulation of Reverse Micelles in Supercritical Carbon Dioxide

Sumeet Salaniwal,[†,‡] Shengting Cui,[†,‡] Hank D. Cochran,[†,‡] and Peter T. Cummings[*,†,‡,§,||]

Departments of Chemical Engineering, Chemistry, and Computer Science, University of Tennessee, Knoxville, Tennessee 37996-2200, and Chemical Technology Division, Oak Ridge National Laboratory, Oak Ridge, Tennessee 37831-6224

We have studied surfactants and reverse micelles in supercritical carbon dioxide (SCO_2) by molecular dynamics simulation using molecular potential models that we have developed for this purpose. In this work we present simulation results suggesting how varying the surfactant molecular architecture and chemistry may affect the structure and properties of reverse micelles in SCO_2. We focus on a dichain surfactant, $(C_7H_{15})(C_7F_{15})CHSO_4^-Na^+$, which forms reverse micelles with aqueous cores in SCO_2.

Introduction

Molecular simulation techniques have significantly contributed toward the understanding of the structure, dynamics, and rheology of aqueous surfactant systems and the relationship of these parameters to surfactant self-assembly, micelles, amphiphilic monolayers and bilayers, and oil solubilization.[1−17] Based on precisely defined molecular models of amphiphilic aggregates, these techniques provide a detailed description of the size, shape, surface roughness, and internal structure of these aggregates. These descriptions can help clarify interpretation of experimental results and establish the significance of assumptions made in theories devised for predicting those structures. In certain conditions where experiments are impractical or impossible (e.g., high temperatures and pressures), molecular simulation techniques can be successfully applied to obtain the much-needed information. The unique advantage of molecular simulation techniques lies in the fact that they provide a direct route from the microscopic details of the system (mass of atoms, intermolecular interaction potential, molecular geometry, etc.) to the macroscopic properties of experimental and fundamental interest. With efficient algorithms and increased computational resources, the scope and capability of these techniques have increased significantly over the past few years and can be expected to increase significantly in the future. A combination of experiment, theory, and simulation has resulted in a sound fundamental knowledge base of micellar systems in aqueous media.

Another class of aggregates is reversed (or inverted) micelles (RMs) in which the roles of the polar and nonpolar parts of the amphiphiles have been reversed and the aqueous microphase is dispersed in a nonpolar solvent. By contrast, the number of molecular simulation studies of such systems has been quite limited. Brown and Clarke[18] reported the first MD simulation of a water-containing model RM in a nonpolar solvent (mimicking *n*-octane). Linse[19] performed a molecular dynamics study of the aqueous core of an ionic RM to investigate the nature of the aqueous core. The system consisted of sodium ions and water molecules, spherically enclosed by a hydrophobic interface carrying carboxylate headgroups. In the only prior study of RM using realistic and detailed models, Tobias and Klein[20] performed a molecular dynamics simulation of a calcium carbonate/calcium sulfonate RM in nonpolar solvents (carbon tetrachloride and octane) and vacuum. The potential model of the surfactant consisted of intra- and intermolecular van der Waals and Coulombic interaction. Harmonic bond stretching, bond angle bending, and dihedral angle potentials were used for intramolecular interactions.

Our interest in RMs comes about through their role in enhancing the solubility of aqueous and polar molecules in SCO_2. Because it is a nontoxic, chemically inert, nonflammable fluid, SCO_2 has been proposed as a preferred solvent substitute in the chemical process industries, but processing of aqueous media or polymers, for example, is hindered by their low solubility in SCO_2. Recently, some promising surfactants have been found that permit colloidal dispersion of aqueous or polymer phases within the cores of RMs in SCO_2. Following promising early reports by Hoefling et al.[21] suggesting the formation of a microemulsion in a surfactant/water/SCO_2 system using surfactant molecules with perfluoropolyether (PFPE) tails, several experimental efforts focused on discovering suitable surfactants that are capable of stabilizing the water/CO_2 interface. The most successful surfactant molecules, identified by these experimental investigations,[22−30] contain fluorinated chains as their CO_2-philic part and various headgroups to support aqueous or polymeric cores. For example, DeSimone and co-workers[22,23] have developed and extensively studied surfactants with CO_2-philic perfluorooctyl acrylate (PFOA) tails and polymeric heads, which thus form a polymeric core and have application in emulsion polymerization. Another class of surfactants known as dichain or hybrid surfactants (surfactants with two tails, one alkane and the other perfluoroal-

* To whom correspondence should be addressed. E-mail: ptc@utk.edu. Phone: +1 865 974 0227. Fax: +1 865 974 4910.
† Department of Chemical Engineering, University of Tennessee.
‡ Oak Ridge National Laboratory.
§ Department of Chemistry, University of Tennessee.
|| Department of Computer Science, University of Tennessee.

10.1021/ie000144m CCC: $19.00
Published on Web 11/15/2000

kane) have been synthesized and shown[27,28] to form RMs with aqueous cores in SCO_2. Johnston and co-workers[26] showed that RMs of dichain surfactants are capable of solubilizing significant amounts of water (approximately 2 wt %) in the RM core, which is about an order of magnitude greater than is possible without surfactants. Although these studies have partially succeeded in identifying some desirable elements of an effective surfactant molecule, they shed limited light on the underlying principles that make these surfactants successful while others are not. Molecular simulation techniques can play an important role in developing an understanding of these principles.

In this work, we have chosen to study the self-aggregation behavior of a dichain (hybrid) surfactant [$(C_7F_{15})(C_7H_{15})CHSO_4^-Na^+$] and water in the presence of carbon dioxide as a nonpolar solvent via molecular dynamics simulation. The dichain surfactant molecule is characterized by the presence of two tails (*n*-alkane tail and *n*-perfluoroalkane tail) attached to an anionic (sulfate) headgroup. The *n*-perfluoroalkane provides the necessary CO_2-philic behavior to the surfactant molecule. In this work, this particular surfactant molecule was chosen for two main reasons. First, in terms of the molecular complexity, this is a relatively small molecule compared to other known CO_2-philic surfactant molecules. Thus, from a computational perspective, it is relatively easy to model this surfactant to a sufficient degree of detail and study the aggregation behavior for a relatively large system size. [Note, however, that on an absolute scale simulations of these systems are computationally challenging and state-of-the-art in terms of size and complexity.] Second, the structural features of RMs formed in the dichain surfactant + water + carbon dioxide ternary system were recently reported by Eastoe and co-workers[27] using small-angle neutron scattering (SANS). Thus, quantitative comparisons with their results can be made.

In the remainder of this paper, we describe the intermolecular models and computational methods used (section 2) and the results from our simulation studies (section 3). We conclude with a summary in section 4. Preliminary results from the simulation study were reported in a recent publication;[31] more detailed results are available in the recent Ph.D. thesis of Salaniwal[32] and additional publications from this thesis.[33,34]

Molecular Models and Simulation Methods

In the system under investigation, there are three chemical components, viz., CO_2 (solvent), water, and surfactant molecules. The rigid model for CO_2 was developed by Harris and Yung[35] and is a potential model with three atomic sites. Each site consists of Lennard-Jones (LJ) interaction and a central point charge. The water molecules were modeled using the rigid modified simple point charge (SPC/E) intermolecular model[36] with one LJ site centered on oxygen and three point charges. The Harris−Yung and SPC/E models were chosen because each well reproduces the experimental critical points and phase envelopes of CO_2 and water, respectively. We constructed the model of the surfactant molecule by assembling existing models for each of the four distinct parts of the molecule (sodium ion, sulfate headgroup, alkane tail, and perfluoroalkane tail), with each part to be modeled explicitly. The intermolecular potentials for the tail groups (alkane and perfluoroalkane) were those of Cui et al.[37,38] for the perfluoroalkane tail and those of Siepmann et al.[39] for the alkane tail. These models for the tails are united-atom models, which represent the CF_3, CF_2, CH_3, and CH_2 groups as pseudo-atoms with LJ interactions only (no electrostatic interactions or polarizibility). The intramolecular interactions within the tails include bond-bending and angle-torsion potentials; the bond lengths are fixed. The model for the sulfate headgroup used was that of Cannon et al.[40] This is a fully atomistic model with a tetrahedral structure, with sulfur at the center and oxygen at the apexes. The sulfur and oxygen sites have charges for Coulombic interactions in addition to LJ interactions. The model for the sodium ion is a single LJ site with a unit positive charge.[14]

Table 1. LJ and Charge Parameters in the Intermolecular Potential Models Used in This Study

atom/site type	σ (Å)	ϵ/κ (K)	q
CH_2 (surfactant tail)	3.93	47	0
CH_3 (surfactant tail)	3.93	114	0
CF_2 (surfactant tail)	4.60	30	0
CF_3 (surfactant tail)	4.60	79	0
sulfur (surfactant headgroup)	3.55	126	+2e
oxygen (surfactant headgroup)	3.15	126	−1e
sodium (surfactant counterion)	2.667	37.65	+1e
hydrogen (water)	0.0	0.0	+0.4238e
oxygen (water)	3.166	78.23	−0.8476e
carbon (CO_2)	2.757	28.129	+0.6512e
oxygen (CO_2)	3.033	80.507	−0.3256e

Hence, the intermolecular potential between two sites is given by the equation

$$u_{ij}(r) = 4\epsilon_{ij}\left[\left(\frac{\sigma_{ij}}{r_{ij}}\right)^{12} - \left(\frac{\sigma_{ij}}{r_{ij}}\right)^{6}\right] + \frac{q_i q_j}{r} \qquad (1)$$

The parameters for each like-site interaction are given in Table 1. Cross-interactions (between unlike atoms) were derived by application of the Lorentz−Berthelot mixing rules to the LJ parameters;[41] Coulombic cross-interactions are given straightforwardly by electrostatics. The simulation codes were parallelized using the replicated data method (also known as the replicated atom method[42]), and the simulations were performed on up to eight processors on the Cray T3E parallel supercomputer at NERSC.

The simulations were performed using molecular dynamics codes developed within our research group. Long-ranged Coulombic interactions were truncated using the site−site reaction field method.[43,44] Bond length constraints were handled using the RATTLE algorithm.[45,46] Two different-sized systems were simulated. To check on the efficacy of the potential models and to explore variations in chain architecture in reasonably short periods of time, we performed simulations on a small system composed of 30 dichain surfactant, 132 water, and 2452 carbon dioxide molecules within a cubic simulation box of length 71.8 Å. The concentrations of the dichain surfactant (0.135 mol/L) and water (0.594 mol/L) molecules used in this small system do not correspond to any particular experimental system but were chosen simply to limit the size of the simulations for exploratory calculations. As a corollary of limiting the system size, a relatively low water-to-surfactant molar ratio ($W_o \sim 4$) is used in this system. Thus, the results pertaining to the structural characteristics of aggregates cannot be expected to be valid for values of W_o greater than the low W_o value used in this system. The solvent conditions used in this system correspond to $T = 310$ K and solvent density = 0.482

g/cm^3. At these state conditions CO_2 is in the near-supercritical state, which should also enhance the surfactant aggregation process. These solvent conditions were chosen to facilitate the study of self-aggregation within a reasonable amount of computer time.

More limited simulations were performed on a large system composed of 33 dichain surfactant, 1175 water, and 12 800 carbon dioxide molecules within a simulation box of length 103.5 Å. This corresponds to 42 618 total interaction sites, which represents one of the largest system sizes used to study surfactant self-assembly via molecular simulation.[31] The concentrations of the surfactant (0.05 mol/L) and water (1.75 mol/L) in this system exactly mimic the concentrations used by Eastoe et al.[27] in their SANS study of this ternary system. The number of surfactant and water molecules used in this large simulation system corresponds to one "average-sized" surfactant aggregate observed in the experimental work. Besides the low concentration of the dichain surfactant molecules in this system, an important difference between this system and the small system is the relatively high water-to-surfactant ratio ($W_o \sim 35$) in this system. The high value of W_o in this system manifests itself as some discernible difference in the dynamics and/or morphology of the aggregates formed in this system compared to those in the small system. The solvent conditions used in this system correspond to $T = 298$ K and solvent density = 0.85 g/cm^3. At these conditions, CO_2 is in a high-temperature liquid state.

Both the small and the large simulations were started from two different initial conditions: an aggregated starting configuration and a scattered starting configuration. The two starting configurations were chosen to test if different starting configurations had any effect on the dynamics of aggregation and/or morphology of the aggregates formed. It should be pointed out that these initial configurations are just two of the infinite possible configurations that can be used and were chosen solely because they were simple and less time-consuming to generate. As shown in Figure 1a, in the aggregated starting configuration for the large system, all of the water molecules were placed within a spherical core at the center of the simulation box. The surfactant molecules with fully extended tails were placed on the surface of the core with their headgroups pointing toward the center. Structurally, this configuration resembles a reversed micellar aggregate and hence the name aggregated starting configuration. In the scattered starting configuration for the large system (Figure 1b), all of the water molecules were scattered within the simulation box and the distance between the surfactant molecules was also increased. In a sense, the two starting configurations represent the two extremes of the system configurations. The scattered starting configuration is a more realistic starting state, while the aggregated starting configuration (especially for the large system) is closer to the desired final state characterized by the presence of a single surfactant aggregate. It is important to mention that the similar starting configurations for the two system sizes are somewhat different (because of different water-to-surfactant ratios), and their effect on the aggregation dynamics and aggregate morphology will be discussed in the following section. For convenience, we will refer to the four kinds of simulations by the following acronyms: SA for small system, aggregated starting configuration; SS for small system, scattered starting configuration; LA for large system, aggregated starting configuration; LS for large system, scattered starting configuration.

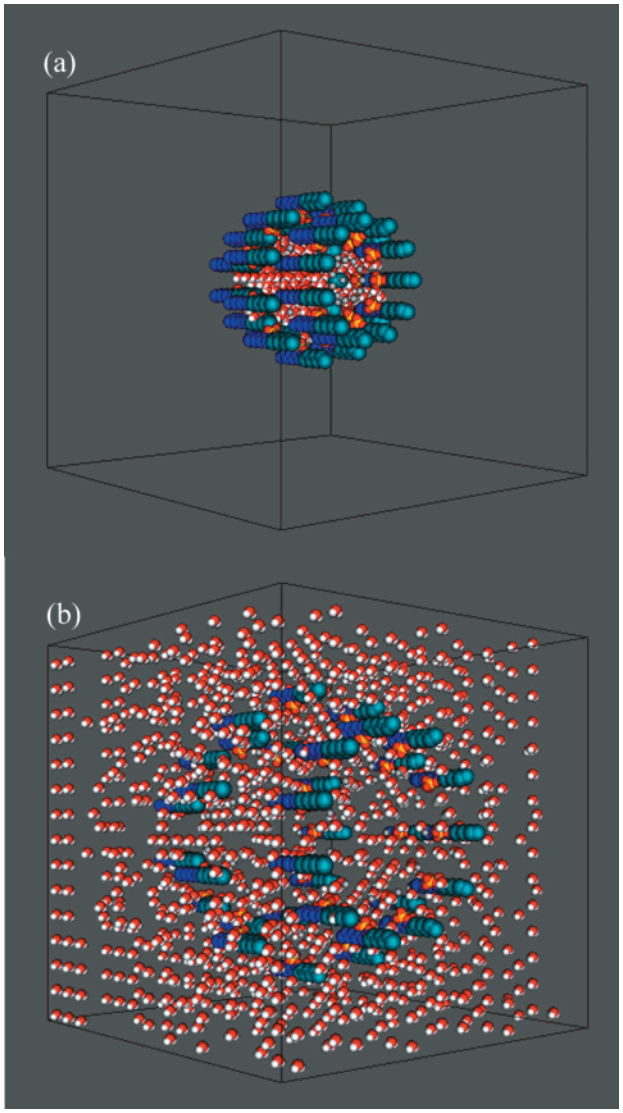

Figure 1. Snapshots of the starting configurations for the large system used in this study: (a) aggregated configuration (SA); (b) scattered configuration (SS). For the small system, the starting configuration looks similar except for having far fewer water molecules. The color scheme of the various species is as follows: light blue for the perfluoroalkane tail, dark blue for the alkane tail, yellow for sulfur, red for oxygen, white for hydrogen, and gray for sodium. CO_2 molecules are not shown for visual clarity.

Results

The aggregation mechanism and dynamics of these systems, as well as the aggregate structure, have recently been discussed in detail elsewhere.[31−34] Here we give a brief summary of these findings to set the stage for a discussion of the effect of chain chemistry and architecture on the aggregation of water and surfactant molecules into RM-like aggregates.

Aggregation Mechanism. The mechanism through which randomly dispersed surfactant molecules spontaneously form stable micellar aggregates is an important aspect of the dynamics of surfactant aggregation. Understanding the mechanism of surfactant aggregation sheds some light on the interactions present in the system that are responsible for holding the surfactant

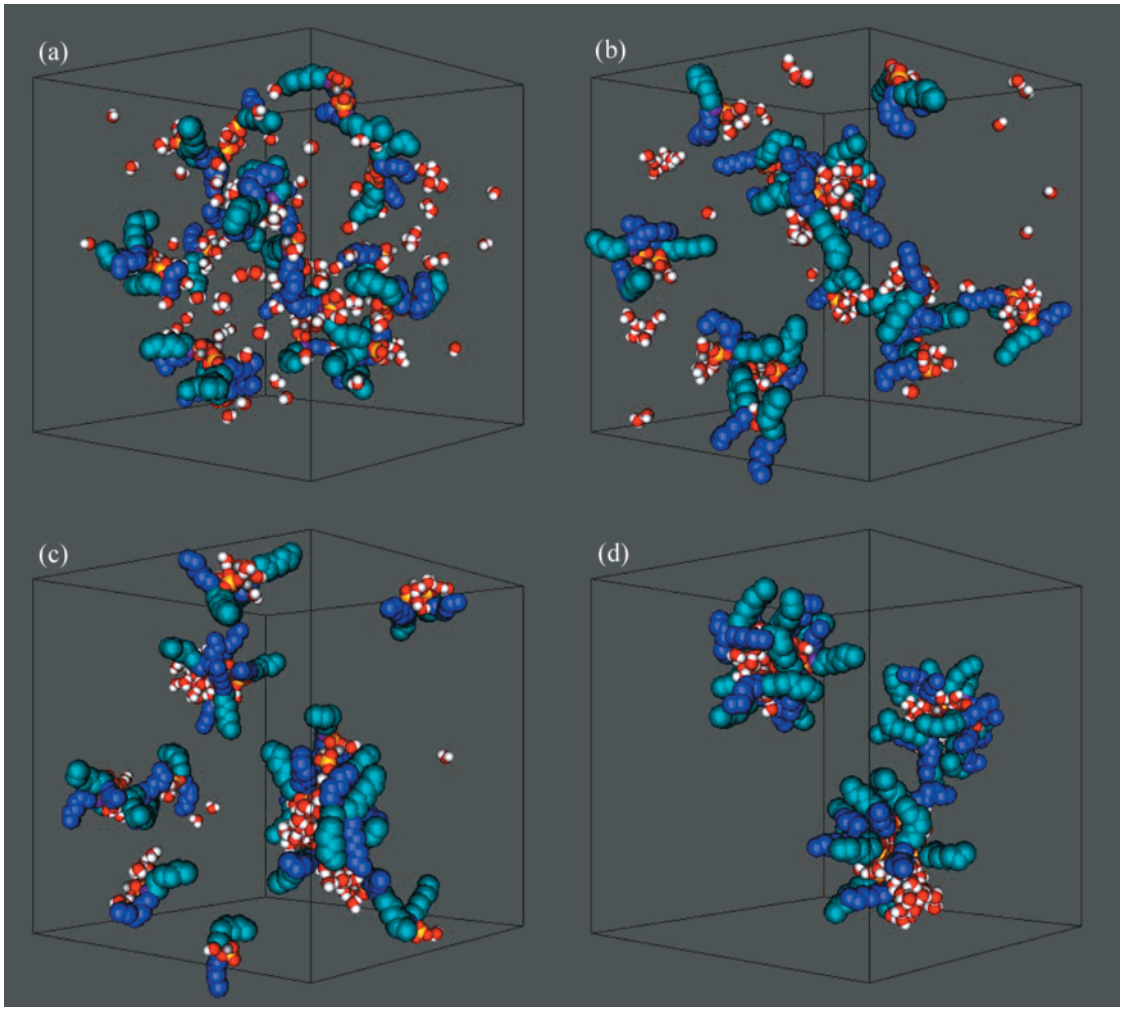

Figure 2. Snapshots of the SA simulation taken at (a) 5.5, (b) 44.6, (c) 148.3, and (d) 1036.0 ps showing the mechanism of surfactant aggregation. The color scheme is the same as that for Figure 1.

molecules together in an aggregate. Parts a−d of Figure 2 show the snapshots of the SA system at various important stages of the aggregation process highlighting the mechanism. A similar aggregation mechanism was observed for the SS system.[34] In all of these snapshots, the solvent molecules are intentionally not shown for reasons of visual clarity. Figure 2a (t = 5.5 ps) shows the system configuration with all of the dichain surfactant and water molecules somewhat randomly dispersed within the simulation box, and no evidence of surfactant aggregation can be observed. The only noticeable fact is that the Na^+ ions and anionic surfactant molecules exist as contact ion pairs. Because the system configuration at this instant appears to have little correlation with the aggregated starting configuration, it can be argued that perhaps the starting configuration has little effect on the long-time dynamics of this system. Figure 2b shows the system configuration at t = 44.6 ps. At this stage a significant number of water molecules have associated themselves with the ionic species present in the system; i.e., the water molecules tend to hydrate the anionic headgroup and Na^+ counterion of the surfactant molecules. Some preliminary evidence of surfactant aggregation is noticeable by the presence of small clusters of hydrated surfactant molecules; however, no appreciable aggregation is evident in the system. The system configuration in Figure 2c (t = 148.3 ps) shows that nearly all of the water molecules are associated with the surfactant molecules and a few small surfactant aggregates have developed in the system, indicating the beginning of surfactant self-assembly. However, no RM-like (an aqueous core surrounded by surfactant molecules with their headgroups immersed in the aqueous core and the tails forming a corona) aggregates are noticeable in the system. After a sufficiently long time (t = 1036.0 ps), the system consists of three roughly similar-sized surfactant aggregates that have the appearance of RMs, as shown in Figure 2d. The water molecules in these aggregates exist in the form of an aqueous core that is well shielded from the surrounding solvent by a layer of surfactant molecules, with their headgroups pointing toward the aqueous core and their tails extending into the solvent. This morphology of the aggregates formed closely resembles that of RMs, indicating the formation of RM-like aggregates in this system.

A careful analysis of the time evolution of the surfactant−surfactant (U_{ss}) and surfactant−water (U_{sw}) interaction energies for the aggregation process[32−34] shows that the aggregation process in both the SA and SS systems appears to follow a two-step aggregation mechanism. The first step involves a rapid (within the first 150 ps) hydration of anionic headgroups and the sodium counterions (that exist as ion pairs prior to hydration) with no appreciable surfactant aggregation. Figure 3, which shows a plot of the fraction of total water molecules associated with surfactant molecules versus time for the SA and SS systems, clearly depicts

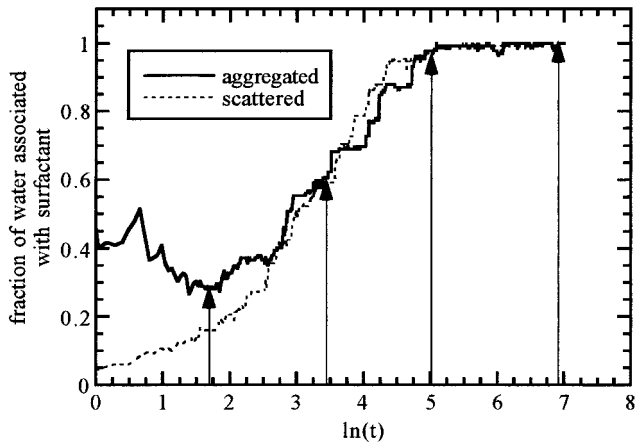

Figure 3. Time evolution of the fraction of water molecules present in the SA and SS systems that are associated with the surfactant molecules. Arrows indicate the times corresponding to the snapshots in Figure 2.

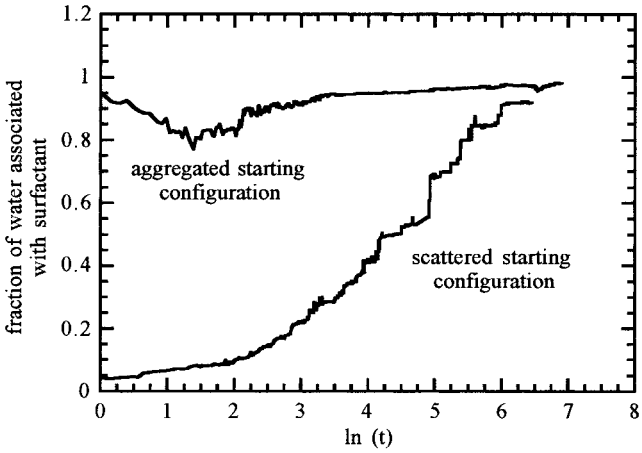

Figure 4. Time evolution of the fraction of water molecules present in the LA and LS systems that are associated with the surfactant molecules.

that the first step primarily involved ion hydration. The figure shows that almost all of the water molecules present in the surfactant system become associated with the sodium ion−anionic surfactant ion pair during the first step and remain associated subsequently. In contrast, the second step of the aggregation process is a much slower step involving gradual aggregation of the hydrated surfactant molecules via hydrogen bond formation into stable RM-like aggregates.

The large system is significantly different from the small system because of its low surfactant concentration, high water-to-surfactant molar ratio, and high solvent density. To investigate the effect of high water-to-surfactant ratio on the large systems, Figure 4 shows the fraction of water molecules associated with surfactant molecules for the LA and LS systems. The curve for the LS system shows an almost linear increase in the fraction of associated water molecules during the interval $\ln(t) \leq 6.0$ ($t \leq 403.4$ ps). This behavior is quite similar to those observed for SA and SS systems (Figure 3), implying that this system also follows the two-step aggregation mechanism (ion hydration followed by surfactant aggregation) shown by the small system. In contrast, the LA system shows that the fraction of molecules associated with surfactant molecules initially decreases, reaches a minimum of ~0.8 at $\ln(t) = 1.5$ ($t = 4.5$ ps), and finally increases gradually with time. This behavior is not only different from that of the SA and SS systems but also different from that of the LS system. This implies that the LA system does not follow the two-step aggregation mechanism, instead its evolution is influenced by its starting configuration. This is attributed to the high W_o in this system because the water molecules in this system are associated with surfactant molecules to begin with. As a result, the ion-hydration step of the aggregation process is not observed in this system. The second aggregation step is also largely absent because of the incomplete dispersion of surfactant and water molecules.

Snapshots of the evolution of the LS system are qualitatively similar to those of the SA and SS systems.[33] In contrast, for the LA system, the system configurations shown in Figure 5a−d (t = 5, 20, 100, and 1000 ps, respectively) show a very different aggregation process. Because of the high water-to-surfactant ratio in this system ($W_o \sim 35$), there is an ineffective dispersion of surfactant and water molecules as monomers or dimers (Figure 5a). Most of the surfactant molecules appear to be connected to each other via water bridges. Subsequently, as seen in Figure 5b,c, the system rapidly reaggregates to form a large aggregate that consists of most of the surfactant and water molecules, while the few remaining surfactant and water molecules form three smaller aggregates. No further aggregation is observed in this system even up to ~1.0 ns, as seen in Figure 5d.

Thus, it can be concluded that the aggregation of dichain surfactant and water molecules in CO_2 essentially follows a two-step mechanism. The first step of this mechanism involves hydration of the anionic surfactant and Na^+ counterions that occurs over $\sim 10^{-10}$ s, while the second step involves gradual ($\sim 10^{-6}-10^{-9}$ s) aggregation of hydrated ions to form stable surfactant aggregates. This two-step mechanism (hydration interaction and subsequent hydrogen bond formation linking the surfactant molecules) for surfactant aggregation has been previously reported by Eicke and co-workers[47] based on the dielectric increment measurements for the system consisting of AOT surfactants in benzene. AOT is an anionic surfactant molecule with two tails and is structurally quite similar to the dichain surfactant molecule studied in this work. Thus, it can be concluded that aggregation of the dichain surfactant in CO_2 is similar to that of other ionic surfactants (namely, AOT) and is essentially governed by the electrostatic interactions between the surfactant headgroups and water molecules. Because the electrostatic interactions are stronger and longer-ranged compared to the hydrophobic interactions[48] that are responsible for aggregation in aqueous solvents, the time scales of aggregation observed in the ternary system under investigation are a few orders of magnitude smaller than those observed for surfactant aggregation in aqueous media.

Aggregation Kinetics. To quantify the progress of self-aggregation in the surfactant system under consideration, we use a measure of the rate of aggregation, which is represented by the slope of the plot of $\ln[N(t)]$ versus $\ln(t)$. Figure 6 shows the plot for the LA and LS systems. The quantity $N(t)$ represents the total number of surfactant aggregates present in the system at any instant of time. It is calculated based on an efficient cluster-counting algorithm proposed by Sevick et al.,[49] according to which if the sites in the water molecules, headgroups, or Na^+ ions (tail groups are not considered)

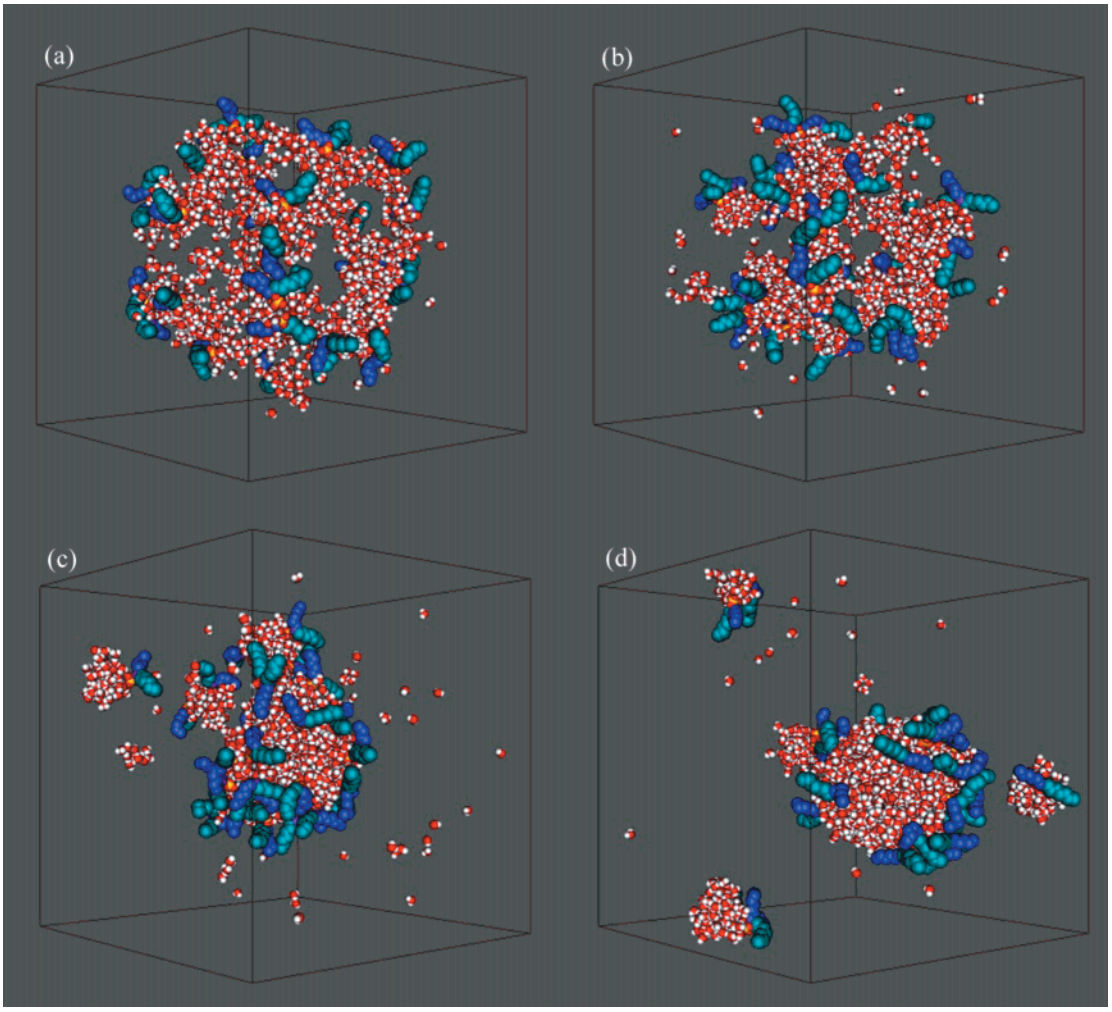

Figure 5. Snapshots of the simulation taken at (a) 5, (b) 20, (c) 100, and (d) 1000 ps showing the mechanism of surfactant aggregation for the LA system. The color scheme is the same as that for Figure 1.

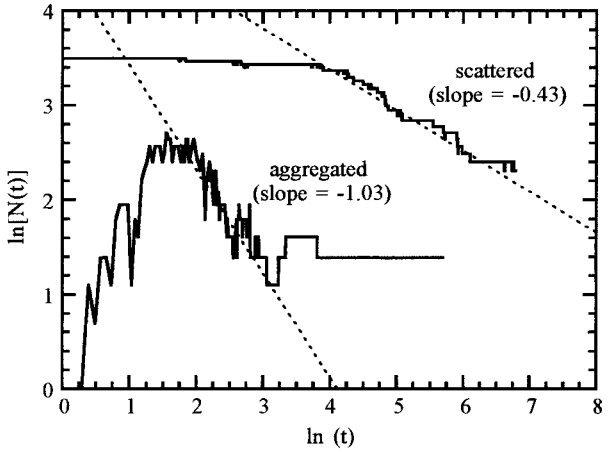

Figure 6. Time evolution of the number of aggregates during the simulation for the C_7-tailed hybrid surfactant in the large system. An aggregate is defined based on the cluster definition of Sevick and co-workers.[49]

of any two molecules lie within a particular distance (3.3 Å in the present case) of each other, then the two particles are considered members of the same cluster. It is assumed that even if a cluster has only one surfactant molecule, it classifies as an aggregate. This definition of an aggregate is somewhat arbitrary and simply adopted for the sake of convenience. Figure 6 shows that $\ln[N(t)]$ has an inverse linear dependence on $\ln(t)$ with a slope of -0.43 for the LS system. If it is assumed that the aggregation curve follows this slope for long times, then the figure suggests that the aggregation process in this system should result in the formation of a single surfactant aggregate consistent with Eastoe et al.[27] in ~200 ns. Unfortunately, the simulation time of ~200 ns is beyond the practical limits of this simulation study. For the LA system, the shape of the aggregation curve in Figure 6 shows a portion with positive slope followed by a portion with negative slope and finally a portion where $\ln[N(t)]$ remains constant. By fitting a straight line through the portion of the aggregation curve with the negative slope, a value of ca. -1.04 is obtained. The higher magnitude of the slope for the LA system is consistent with the fact that this system is much closer to the expected final state (a single surfactant aggregate as observed by Eastoe et al.[27]) compared to the LS system.

The inverse linear dependence over a limited range of time implies that the aggregation behavior can be well represented by a scaling relation of the form $N(t) \sim t^{-z}$, where z is the absolute value of the slope of the aggregation curve. This type of aggregation behavior is consistent with Smolouchowski's theory of diffusion-limited aggregation (DLA),[50] according to which the rate of aggregation in the system under investigation is dependent on the concentration of the aggregating particles and their diffusivity. More detail concerning

Table 2. Comparison between Characteristics of the Large RM-like Aggregate in the SA System with Neutron Scattering Results of Eastoe et al. at the Same Conditions

	this work	SANS experiments
water	916 ± 10	
surfactant	26	
W_o	35.2	35
R_g (Å)	15.4 ± 0.2	20.5 ± 1.0
I_{max}/I_{min}	1.3 ± 0.1	
η	0.12 ± 0.05	
A_s (Å^2)	115 ± 3	140

the applicability of the ideas of DLA to the self-assembly of these water/surfactant aggregates can be found elsewhere.[34] It suffices to say here that two effects have been shown to be important in these systems: diffusion of the aggregates and steric hindrance to aggregation caused by the perfluoroalkyl chains. The latter effect manifests itself in the fact that many collisions between aggregates do not result in merging of the two aggregates because of the presence of the perfluoroalkyl chains.

Structure of Aggregates. As mentioned earlier, one of the reasons for choosing to simulate the dichain surfactant + water + carbon dioxide system was to make quantitative comparisons with the SANS study of Eastoe et al.[27] on the same system. Table 2 provides the structural properties of the largest aggregate formed in the LA system (Figure 5d), because this represents the closest configuration to the expected final state. The simulations show that the aqueous core of the largest aggregate seen in Figure 5d has a radius of gyration (R_g) of 15.4 ± 0.3 Å. This is in a reasonably good agreement with the experimentally determined value of 20.5 ± 1.0 Å. From the simulations, the shape of the aqueous core was quantified using the ratio of the largest to the smallest principal moments of inertia (I_{max}/I_{min}) and the eccentricity (η). The eccentricity is calculated by the equation

$$\eta = 1 - I_{min}/I_{avg} \qquad (2)$$

where I_{avg} is the average of all three components of the principal moment of inertia. Both of these parameters provide a measure of the deviation from a perfectly spherical object ($I_{max}/I_{min} = 1$ and $\eta = 0$), and the uncertainty in their values reflects the effect of the spatial or temporal fluctuations in the shape of the aqueous core. The value of $I_{max}/I_{min} = 1.2 \pm 0.1$ and $\eta = 0.1 \pm 0.05$ (no experimental data available indicate that the aggregate is nearly spherical with small fluctuations). This is expected because of the high water-to-surfactant ratio ($W_o \sim 35$) in this aggregate. The high W_o values result in the aqueous core of large volume (and surface area) that facilitates a reasonably low packing density of surfactant molecules around the aqueous core. Experimentally, Eastoe et al.[27] used the parameter A_s (surface area of the aqueous core per surfactant molecule) to characterize the shape of the aqueous core. The parameter A_s is given by the equation

$$A_s = 4\pi R_g^2/N_s \qquad (3)$$

where N_s is the aggregation number (number of surfactant molecules in the aggregate). In essence, this quantity is a measure of the packing density of the surfactant molecules in the aggregate and, thus, can be related to the shape of its aqueous core. The value of A_s for the aggregate estimated from the simulation is 115 Å^2, which is in approximate agreement with the experimentally reported value of 140 Å^2. For surfactant aggregates formed in the SA system (Figure 2d), the structural properties are influenced by the low water-to-surfactant ratio ($W_o \sim 4$) in this system. The results indicate that the I_{max}/I_{min} values for all three aggregates are significantly greater than unity and the η values are significantly greater than zero. Thus, the aggregates formed are highly nonspherical compared to those formed in the large system.

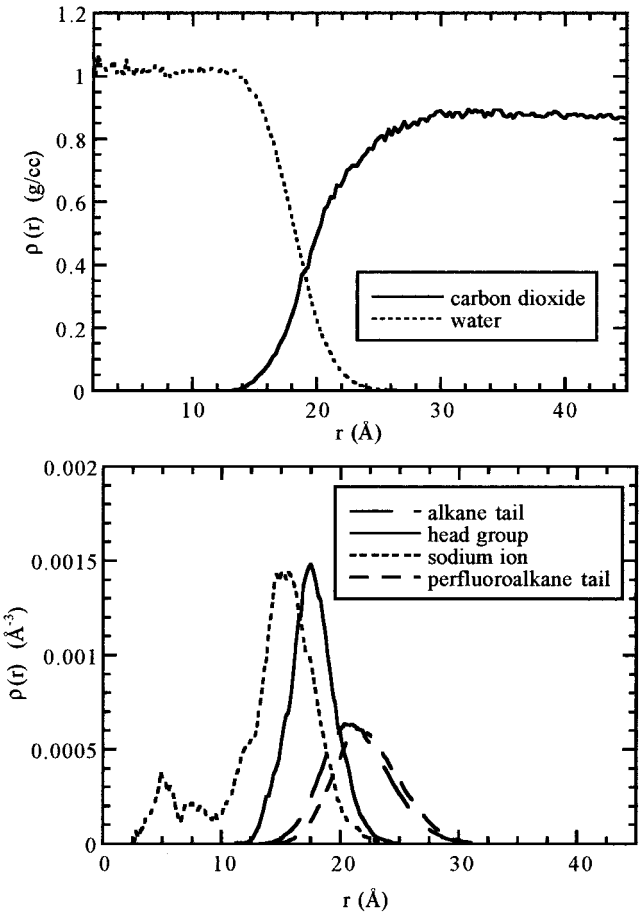

Figure 7. Structural properties of the aggregate formed in the LA system: (a, top) interfacial region; (b, bottom) microstructure of the surfactant molecule.

The microstructure of the aggregates is explored using the singlet distribution function (singlet radial density) profiles of the various atomic groups or molecules constituting the aggregate. The singlet distribution function is a time-averaged measure of the distribution of an atom or molecule from the center of mass of the aqueous core. It is calculated by the equation

$$\rho(r) = \langle N(r) \rangle / 4\pi r^2 \Delta r \qquad (4)$$

where $\langle N(r) \rangle$ is the time average of the number of an atom or molecule that is found in a shell of thickness Δr at a radial distance r from the reference point. Parts a and b of Figure 7 show the microscopic details of the largest aggregate formed in the LA system (Figure 5d). Figure 7a shows that the aqueous core consists of water at ~1.0 g/cm^3, indicating the presence of bulklike water and negligible solvent penetration. The radial density distribution in Figure 7b shows that the headgroups lie at the surface of the aqueous core, with the Na^+ ions

residing within the aqueous core and ion-paired to the anionic headgroups. The distribution of the two tails suggests that the tails form the corona of the aggregate.

The contrasting CO_2-philic behavior of the two tail groups is manifested by the extent of their fully extended conformation. The perfluoroalkane tails have an average of 90 ± 2% trans conformation compared to 74 ± 5% for the alkane tails. Interestingly, the behavior of the two tails is quite opposite in vacuo. The perfluoroalkane tail has a trans conformation of 80% in vacuo compared to 89% for the alkane tail. This contrasting behavior of the two tails implies that in the presence of CO_2 as a solvent medium the perfluoroalkane tails assume more extended conformations than the alkane tails and is a measure of their CO_2-philic behavior.

Effect of Tail Chemistry. As mentioned earlier, little is known at present about the ingredients of a successful CO_2-philic surfactant. For instance, in the dichain surfactant molecule the perfluoroalkane tail provides the required CO_2-philic property, while the role of the alkane tail is not so clear. One possible explanation could be to provide the surfactant the required architecture,[51] enabling it to form RM-like aggregates on self-assembly. However, it is not known what surfactant chemistry provides the optimum aggregation properties to the dichain surfactant. In other words, what should be the balance between the perfluoroalkane and the alkane tails for an effective surfactant molecule? This is important in determining solubility characteristics of the surfactant molecule. To gain some insight into the role played by each of the two functionally distinct tails on surfactant self-aggregation and aggregate morphology, two independent simulations of the SA system were performed. Although the small system does not correspond to any experimental composition, it was chosen for the sake of computational economy. The simulations of the large system are computationally expensive, and only a few such simulations can be performed. As shown earlier, the results of the small system give a reasonably good prediction of the aggregation dynamics; thus, it is expected that these simulations can provide some useful qualitative insight. In one simulation, both of the tails of the dichain surfactant were made perfluoroalkane tails (referred to as fully fluorinated surfactant), while in the other case, both of the tails were made alkane tails (referred to as the fully hydrogenated surfactant); i.e., the fully fluorinated surfactant had both tails CO_2-philic, while the fully hydrogenated surfactant molecule had none. However, changing the chemical characteristics of the dichain surfactant from hybrid to fully fluorinated (or fully hydrogenated) also changes the molecular mass of the molecule quite significantly. In comparison to the hybrid surfactant, the fully fluorinated surfactant has a higher molecular weight (M_w = 870 g/mol), while the fully hydrogenated surfactant has a much lower molecular weight (M_w = 330 g/mol). Because the aggregation dynamics observed in the surfactant system under investigation is diffusion-limited, it is expected that the significant difference in the molecular mass of fully fluorinated and fully hydrogenated surfactants should have considerable influence on the rate of aggregation of these systems. Figure 8 shows the mean-squared displacement (MSD) curves for the two different surfactant molecules during the first 100 ps of the aggregation process. As expected, the slope of the MSD curve for the fully fluorinated surfactant molecules is significantly lower (indicating slower diffusion) compared to that of the fully hydrogenated surfactant. The different diffusional characteristics of the fully fluorinated and fully hydrogenated surfactants also manifest themselves in the differences in their aggregation curves, as shown in Figure 9. The aggregation curve for the fully fluorinated surfactant is ~1 ln(t) units to the right of that for the fully hydrogenated surfactant, implying that, for a similar starting configuration, the fully hydrogenated surfactants exhibit more rapid aggregation compared to the fully fluorinated surfactants. Also shown on this figure are the aggregation curves for no surfactant molecules (i.e., water + SCO_2) and for the dichain surfactant. The dynamics of the system containing fully fluorinated surfactants is not that different from that of the hybrid dichain surfactant and can be seen to be slightly slower for the fully fluorinated surfactant system. In the absence of any surfactant, the water aggregates most rapidly, corresponding to a phase separation into a water-rich and carbon dioxide-rich phase. The solubility of water in the carbon dioxide-rich phase is approximately the same as that measured experimentally at these state conditions. In the short term, the fully hydrogenated surfactant system follows the dynamics of the hybrid dichain system, before switching to a more rapid aggregation dynamics; at later times, the dynamics of the fully fluorinated surfactant system follows that of the hybrid dichain system. This suggests that the early time dynamics, associated with the rapid (within the first 150 ps) hydration of anionic headgroups and the sodium counterions (which exist as ion pairs prior to hydration), is not appreciably affected

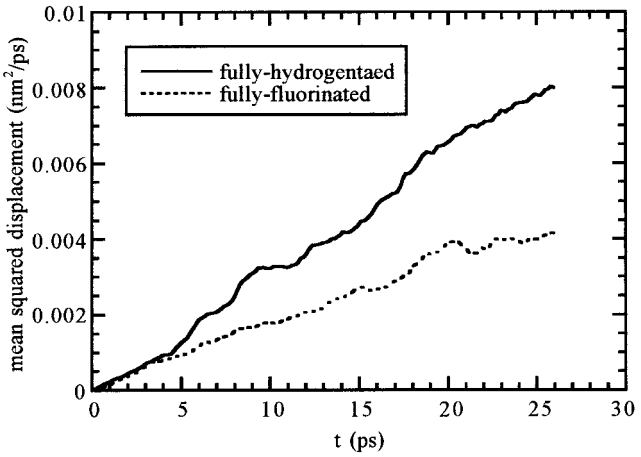

Figure 8. MSD of the C_7-tailed fully fluorinated and C_7-tailed fully hydrogenated surfactants during the first 80 ps of the aggregation process.

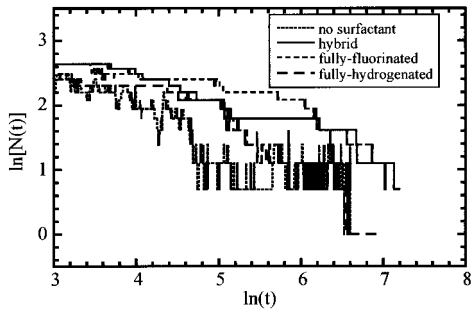

Figure 9. Time evolution of the number of aggregates during the simulation for the C_7-tailed fully fluorinated and C_7-tailed fully hydrogenated surfactant, compared to the evolution for the hybrid dichain surfactant and no surfactant.

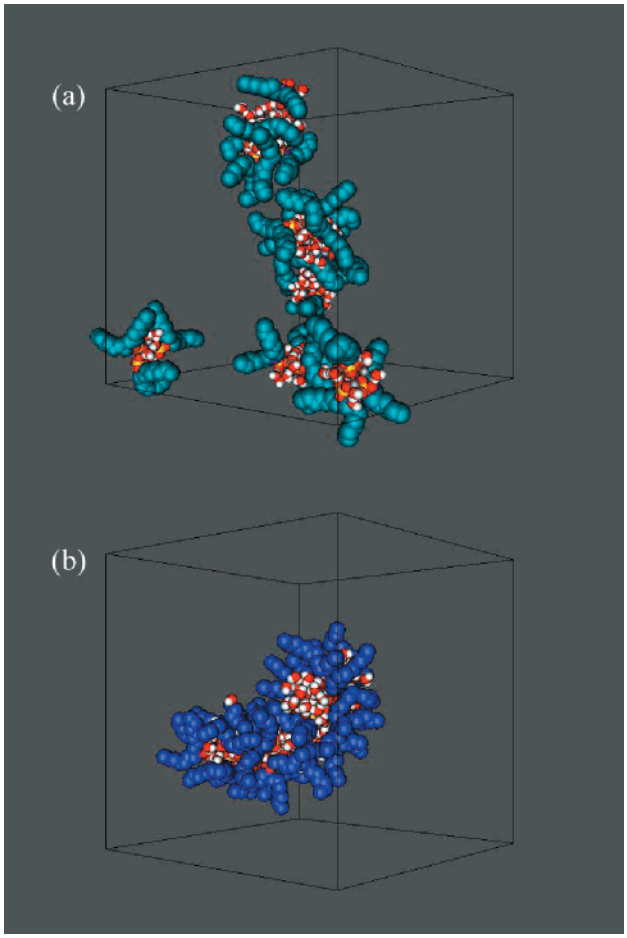

Figure 10. Snapshots of the system configuration for (a) the C_7-tailed fully fluorinated surfactant and (b) the C_7-tailed fully hydrogenated surfactant, after ~1.2 ns.

by the tail chemistry. However, the second stage ($\ln(t) > 5$, $t > 150$ ps), which is dominated by the merging of aggregates, is significantly affected by the chain chemistry, with the fluorinated tail playing an important role of limiting the rate of aggregation. Although these results have been found on a small, artificial system, it suggests that the perfluorinated tail (whether in a dichain surfactant or in a fully fluorinated surfactant) plays a crucial role in preventing aggregation into a separate phase and so may be responsible for the dispersion of the water into RMs.

The difference in surfactant chemistry of the two surfactants is also reflected in the different packing characteristics of these surfactant molecules within an aggregate. This is manifested as a difference in the structural properties of aggregates formed in the two simulations. Parts a and b of Figure 10 show the snapshots (at ~1.2 ns) of the system configuration for the fully fluorinated and the fully hydrogenated surfactant molecules, respectively. It should be stated that these configurations are only valid for the value of $W_o \sim 4$ used in these two systems. Within the simulation time of ~1.2 ns, the fully fluorinated surfactant molecules form five aggregates, while the fully hydrogenated surfactant molecules form a single aggregate. If formation of a single surfactant aggregate is assumed to be the expected final state, then clearly the system with fully hydrogenated surfactants exhibits more rapid aggregation than fully fluorinated surfactants. The difference in the configurations of the two systems, as

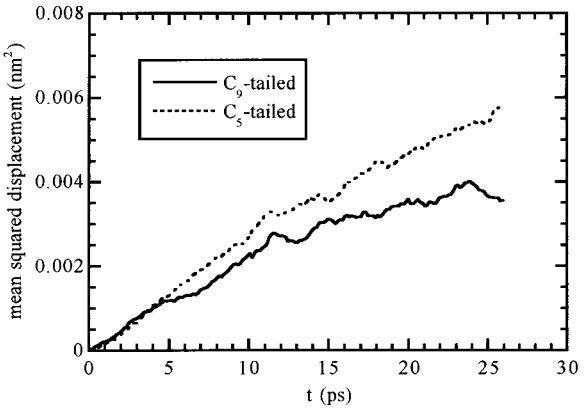

Figure 11. MSD of the C_5-tailed and C_9-tailed hybrid surfactants during the first 80 ps of the aggregation process.

shown in Figure 10a,b, could also be attributed to the more extended perfluoroalkane tails. This should result in higher steric resistances experienced by the fully fluorinated surfactants compared to the fully hydrogenated surfactants.

Effect of Tail Length. Besides the effect of surfactant chemistry on self-aggregation, another factor that significantly affects aggregation in nonpolar solvents is the length of the surfactant tail groups. In fact, this has been the subject of numerous experimental studies[52,53] on different surfactant molecules. The general conclusion of these studies has been that surfactant tails play a very important role in determining the size and shape of RM aggregates. However, little is known regarding the effect of surfactant tail length on the dynamics of aggregation in nonpolar solvents. In an effort to design new CO_2-philic surfactants, it is important to know what surfactant tail lengths provide optimum surfactant architecture. Thus, to gain some basic insight into this aspect, two independent simulations of the small system were performed. Again, the small systems were chosen because of their computational simplicity. In one of these simulations, the length of each tail of the surfactant molecule was reduced by two functional groups (i.e., a C_5-tailed hybrid surfactant was used), while in the other, a two-unit longer tail (i.e., a C_9-tailed surfactant) was used. Figure 11 shows the MSD of the surfactant molecules during the first 80 ps of the aggregation process, during which most of the surfactant molecules are in the dispersed state. The figure shows that the difference in the MSD curves for the two different surfactant molecules is considerably less than that observed by changing surfactant chemistry (Figure 8). This is somewhat expected because the molecular weights of the two surfactants are relatively close to each other ($M_w = 472$ g/mol for the C_5-tailed surfactant compared to $M_w = 728$ g/mol for the C_9-tailed surfactant). Hence, it is expected that the dynamics of aggregation in these two simulations should be quite similar too. Figure 12 shows the aggregation curves for both of the surfactant molecules. As expected, the aggregation curves for the two different surfactant molecules are quite similar. Both of the surfactant molecules exhibit diffusion-limited aggregation behavior with similar slopes. Thus, changing the surfactant tail length appears to have a small effect on the dynamics of aggregation for the surfactant system under consideration.

Parts a and b of Figure 13 show the snapshots of the system of the C_5-tailed surfactant and the C_9-tailed surfactant, respectively, at ~1.1 ns. Both systems show

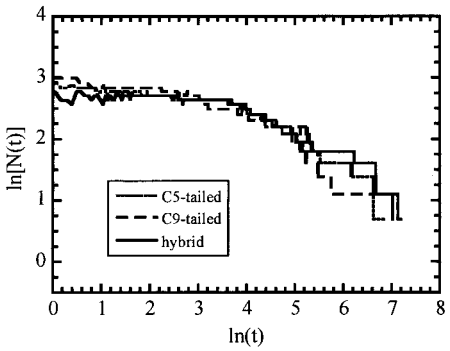

Figure 12. Time evolution of the number of aggregates during the simulation for the C_7-tailed fully fluorinated surfactant system and the C_7-tailed fully hydrogenated surfactant system. The evolution of the hybrid dichain surfactant system is shown for comparison.

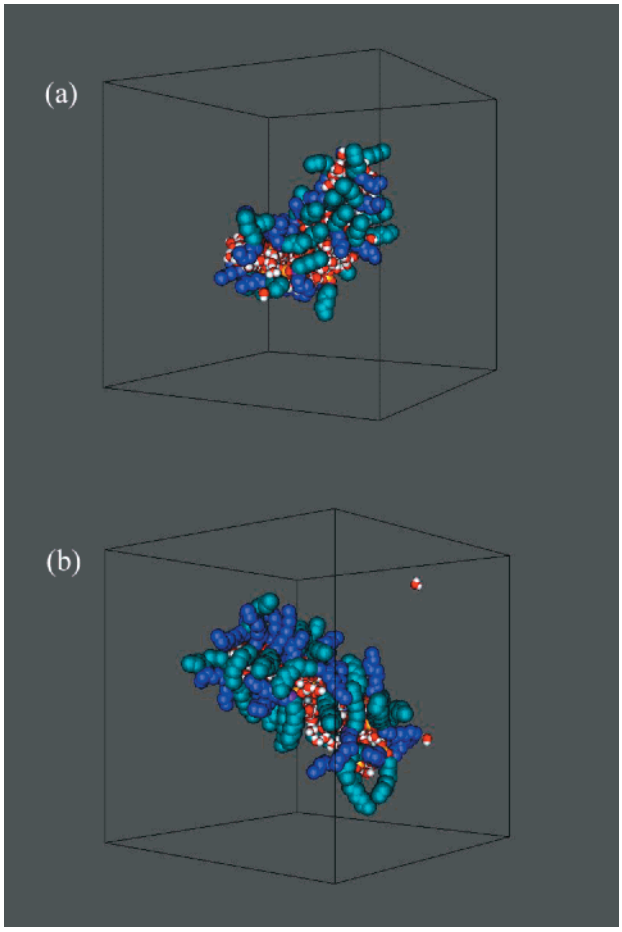

Figure 13. Snapshots of the system configuration for (a) the C_5-tailed hybrid surfactant and (b) the C_9-tailed hybrid surfactant, after ~1.1 ns.

the formation of a single surfactant aggregate within the time interval. The aggregates formed in both cases appear to be highly nonspherical. However, the extent of nonsphericity in the C_9-tailed surfactant appears to be much higher than that in the C_5-tailed surfactant. The aggregate formed from the C_5-tailed surfactant has an eccentricity of 0.5 ± 0.1 compared to 0.9 ± 0.2 for the aggregate formed from the C_9-tailed surfactant. Although the eccentricity of the aggregates in both cases may be due to the low water-to-surfactant ratio ($W_o \sim 4$), the exceptionally large nonsphericity of the aggregate of the C_9-tailed surfactant could be due to the longer tails of this surfactant molecule. Thus, the tail groups of the C_9-tailed surfactant experience stronger steric resistances, thereby resulting in a packing geometry that is highly nonspherical, especially for the low W_o used in this system.

Conclusions

The objective of this research work was to study the self-assembly of dichain surfactant and water molecules in carbon dioxide (solvent) via molecular dynamics simulations to develop a molecular level insight into desirable properties of an effective CO_2-philic surfactant. The simulations presented here involved two different system sizes, each with two different starting configurations. The SA and SS systems represent the system for exploratory calculations, while the LS and LA systems mimic the experimental system of Eastoe et al.[27] The results of the simulation reveal a rapid and spontaneous aggregation of dichain surfactant and water molecules into RM-like aggregates. The aggregation process follows a two-step mechanism, similar to those observed for similar surfactants (namely, AOT) in other nonpolar solvents. In general, the time scales of the two steps are a few orders of magnitude smaller than those observed in aqueous surfactant systems and could be attributed to long-range electrostatic interactions responsible for aggregation in the system under investigation.

A measure of the rate of aggregation is estimated by the time evolution of $\ln[N(t)]$ versus $\ln(t)$, where $N(t)$ is the number of surfactant aggregates present in the system. The results show that the aggregation behavior could be well represented by a relationship of the form $N(t) \sim t^{-z}$, where z is the measure of the rate of aggregation. This behavior is consistent with Smoluchowski's theory of diffusion-limited aggregation. Another factor that is observed to play an important role in aggregation kinetics is the steric resistances offered by surfactant tails, which results in slowing down the aggregation process.

The structural properties of the surfactant aggregate formed in the LA system (closest to the expected final state) are in reasonably good agreement with the experimentally determined values.[27] This suggests that the molecular models and the simulation methodology adopted in this work are adequate to study the aggregation of dichain surfactant molecules. The microstructure of the aggregate revealed the presence of an aqueous core with bulklike water density. The surfactant headgroups and Na^+ ions reside at the interface, and the tails form the corona.

The effects of surfactant chemistry and architecture reveal interesting insights into the aggregation process. For the effect of surfactant chemistry, the fully fluorinated surfactants exhibit slower aggregation kinetics and higher steric resistances. For the effect of tail length, the aggregation kinetics are similar for the shorter-tailed and longer-tailed dichain surfactant; however, considerable differences in the aggregate shape are observed.

Literature Cited

(1) Haan, S. W.; Pratt, L. R. Monte Carlo Study of a Simple Model for Micelle Structure. *Chem. Phys. Lett.* **1981**, *79*, 436−440.

(2) Owenson, B.; Pratt, L. R. Molecular Statistical Thermodynamics of Model Micellar Aggregates. *J. Phys. Chem.* **1984**, *88*, 2905−2915.

(3) Haile, J. M.; O'Connell, J. P. Internal Structure of a Model Micelle via Computer Simulation. *J. Phys. Chem.* **1984**, *88*, 6363−6366.

(4) Woods, M. C.; Haile, J. M.; O'Connell, J. P. Internal Structure of a Model Micelle via Computer Simulation. 2. Spherically Confined Aggregates with Mobile Headgroups. *J. Phys. Chem.* **1985**, *90*, 1875−1885.

(5) Karaborni, S.; O'Connell, J. P. Molecular Dynamic Simulations of Model Micelles. 4. Effects of Chain Length and Headgroup Characteristics. *J. Phys. Chem.* **1990**, *94*, 2624−2631.

(6) Karaborni, S.; O'Connell, J. P. Molecular Dynamic Simulations of Model Micelles. 3. Effects of Various Intermolecular Potentials. *Langmuir* **1990**, *6*, 905−911.

(7) Karaborni, S.; O'Connell, J. P. Molecular Dynamics Simulations of Model Chain Molecules and Aggregates including Surfactants and Micelles. *Tenside, Surfactants, Deterg.* **1993**, *30*, 235−242.

(8) Smit, B.; Hilbers, P. A. J.; Esselink, K.; Rupert, L. A. M.; van Os, N. M.; Schlijper, A. G. Computer simulations of a water/oil interface in the presence of micelles. *Nature* **1990**, *348*, 624−625.

(9) Smit, B.; Hilbers, P. A. J.; Esselink, K.; Rupert, L. A. M.; van Os, N. M.; Schlijper, A. G. Structure of a Water/Oil Interface in the Presence of Micelles: A Computer Simulation Study. *J. Phys. Chem.* **1991**, *95*, 6361−6368.

(10) Smit, B.; Esselink, K.; Hilbers, P. A. J.; van Os, N. M.; Rupert, L. A. M.; Szleifer, I. Computer Simulations of Surfactant Self-Assembly. *Langmuir* **1993**, *9*, 9−11.

(11) Karaborni, S.; van Os, N. M.; Esselink, K.; Hilbers, P. A. J. Molecular Dynamics Simulations of Oil Solubilization in Surfactant Solutions. *Langmuir* **1993**, *9*, 1175−1178.

(12) Karaborni, S.; Esselink, K.; Hilbers, P. A. J.; Smit, B.; Karthauser, J.; van Os, N. M.; Zana, R. Simulating the Self-Assembly of Gemini (Dimeric) Surfactants. *Science* **1994**, *266*, 254−256.

(13) Watanabe, K.; Ferrario, M.; Klein, M. L. Molecular Dynamics Study of a Sodium Octanoate Micelle in Aqueous Solution. *J. Phys. Chem.* **1988**, *92*, 819−821.

(14) Jonsson, B.; Edholm, O.; Telleman, O. Molecular dynamics simulations of a sodium octanoate micelle in aqueous solution. *J. Chem. Phys.* **1986**, *85*, 2259−2271.

(15) Shelley, J. C.; Sprik, M.; Klein, M. L. Molecular Dynamics Simulation of an Aqueous Sodium Octanoate Micelle using Polarizable Surfactant Molecules. *Langmuir* **1993**, *9*, 916−926.

(16) Mackie, A. D.; Panagiotopoulos, A. Z.; Szleifer, I. Aggregation Behavior of a Lattice Model for Amphiphiles. *Langmuir* **1997**, *13*, 5022−5031.

(17) Floriano, M. A.; Caponetti, E.; Panagiotopoulos, A. Micellization in Model Surfactant Systems. *Langmuir* **1999**, *15*, 3143−3151.

(18) Brown, D.; Clarke, J. H. R. Molecular Dynamics Simulation of a Model Reverse Micelle. *J. Phys. Chem.* **1991**, *92*, 2881−2888.

(19) Linse, P. Molecular dynamics study of the aqueous core of a reversed ionic micelle. *J. Chem. Phys.* **1989**, *90*, 4992−5004.

(20) Tobias, D. J.; Klein, M. L. Molecular Dynamics Simulations of a Calcium Carbonate/Calcium Sulfonate Reverse Micelle. *J. Phys. Chem.* **1996**, *100*, 6637−6648.

(21) Hoefling, T. A.; Enick, R. M.; Beckman, E. J. Microemulsions in Near-Critical and Supercritical CO_2. *J. Phys. Chem.* **1991**, *95*, 7127−7129.

(22) DeSimone, J. M.; Guan, Z.; Elsbernd, C. S. Synthesis of Fluoropolymers in Supercritical Carbon Dioxide. *Science* **1992**, *257*, 945−947.

(23) DeSimone, J. M.; Maury, E. E.; Menceloglu, Y. Z.; McClain, J. B.; Romack, T. J.; Combes, J. R. Dispersion Polymerizations in Supercritical Carbon Dioxide. *Science* **1994**, *265*, 356.

(24) Fulton, J. L.; Pfund, D. M.; McClain, J. B.; Romack, T. J.; Maury, E. E.; Combes, J. R.; Samulski, E. T.; DeSimone, J. M.; Capel, M. Aggregation of Amphiphilic Molecules in Supercritical Carbon Dioxide: A Small-Angle X-ray Scattering Study. *Langmuir* **1995**, *11*, 4241−4249.

(25) Cooper, A. I.; Londono, D.; Wignall, G.; McClain, J. B.; Samulski, E. T.; Lin, J. S.; Dobrynin, A.; Rubinstein, M.; Burke, A. L. C.; Frechet, J. M. J.; DeSimone, J. M. Liquid−Liquid Extractions Using Dendrimer-Modified Carbon Dioxide. *Nature* **1997**, *389*, 368−371.

(26) Johnston, K. P.; Harrison, K. L.; Clarke, M. J.; Howdle, S. M.; Heitz, M. P.; Bright, F. V.; Carlier, C.; Randolph, W. Water-in-Carbon Dioxide Microemulsions: An Environment for Hydrophiles Including Proteins. *Science* **1996**, *271*, 624−626.

(27) Eastoe, J.; Bayazit, Z.; Martel, S.; Steytler, D. C.; Heenan, R. K. Droplet Structure in a Water-in-CO_2 Microemulsion. *Langmuir* **1996**, *12*, 1423−1424.

(28) Harrison, K. L.; Goveas, J.; Johnston, K. P.; O'Rear, E. A. Water-in-Carbon Dioxide Microemulsions with a Fluorocarbon−Hydrocarbon Hybrid Surfactant. *Langmuir* **1994**, *10*, 3536−3541.

(29) Beckman, E. J. Carbon Dioxide Extraction of Biomolecules. *Science* **1996**, *271*, 613−614.

(30) McClain, J. B.; Betts, D. E.; Canelas, D. A.; Samulski, E. T.; DeSimone, J. M.; Londono, J. D.; Cochran, H. D.; Wignall, G. D.; Chillura-Martino, D.; Triolo, R. Design of Nonionic Surfactants for Supercritical Carbon Dioxide. *Science* **1996**, *274*, 2049−2052.

(31) Salaniwal, S.; Cui, S. T.; Cummings, P. T.; Cochran, H. D. Self-Assembly of Reverse Micelles in Water/Surfactant/Carbon Dioxide Systems by Molecular Simulation. *Langmuir* **1999**, *15*, 5188−5192.

(32) Salaniwal, S. Self-Assembly of Di-Chain Surfactant in Carbon Dioxide. Ph.D. Thesis, University of Tennessee, Knoxville, TN, 2000.

(33) Salaniwal, S.; Cui, S. T.; Cochran, H. D.; Cummings, P. T. Self-assembly in a dichain surfactant/water/carbon dioxide system via molecular simulation. I. Structural properties of surfactant aggregates. *Langmuir* **2000**, in press.

(34) Salaniwal, S.; Cui, S. T.; Cochran, H. D.; Cummings, P. T. Self-assembly in a dichain surfactant/water/carbon dioxide system via molecular simulation. II. Aggregation dynamics. *Langmuir* **2000**, in press.

(35) Harris, J. G.; Yung, K. H. Carbon Dioxide's Liquid−Vapor Coexistence Curve and Critical Properties as Predicted by a Simple Molecular Model. *J. Phys. Chem.* **1995**, *99*, 12021−12024.

(36) Berendsen, H. J. C.; Grigera, J. R.; Straatsma, T. P. The Missing Term in Effective Pair Potentails. *J. Chem. Phys.* **1987**, *91*, 6269−6271.

(37) Cui, S. T.; Siepmann, J. I.; Cochran, H. D.; Cummings, P. T. Intermolecular potentials and vapor−liquid-phase equilibria of perfluorinated alkanes. *Fluid Phase Equilib.* **1998**, *146*, 51−61.

(38) Cui, S. T.; Cochran, H. D.; Cummings, P. T. Vapor−liquid-phase coexistence of alkane carbon dioxide and perfluoralkane carbon dioxide mixtures. *J. Phys. Chem.* **1999**, *103*, 4485−4491.

(39) Siepmann, J. I.; Karaborni, S.; Smit, B. Simulating the critical behavior of complex fluids. *Nature* **1993**, *365*, 330−332.

(40) Cannon, W. R.; Pettitt, B. M.; McCammon, J. A. Sulfate Anion in Water: Model Structural, Thermodynamic, and Dynamic Properties. *J. Phys. Chem.* **1994**, *98*, 6225−6230.

(41) Allen, M. P.; Tildesley, D. J. *Computer Simulation of Liquids*; Clarendon Press: Oxford, 1994.

(42) Plimpton, S. Fast Parallel Algorithm for short-range molecular dynamics. *Comput. Phys.* **1995**, *117*, 1−19.

(43) Steinhauser, O. Reaction field simulation of water. *Mol. Phys.* **1982**, *45*, 335−348.

(44) Hummer, G.; Soumpasis, D. M.; Newmann, M. Pair correlations in an NaCl−SPC water model: Simulations versus extended RISM computations. *Mol. Phys.* **1992**, *77*, 769−785.

(45) Andersen, H. C. Rattle: a velocity verlet version of the shake algorithm for molecular dynamics calculations. *J. Comput. Phys.* **1983**, *52*, 24−34.

(46) Ciccotti, G.; Ferrario, M.; Ryckaert, J. P. Molecular dynamics of rigid systems in Cartesian coordinates: A general formulation. *Mol. Phys.* **1982**, *47*, 1253−1264.

(47) Eicke, H. F.; Christen, H. Is Water Critical to the Formation of Micelles in Apolar Media. *Helv. Chim. Acta* **1978**, *61*, 2258−2263.

(48) Tanford, C. *The Hydrophobic Effect: Formation of Micelles and Biological Membranes*; Wiley-Interscience: New York, 1973.

(49) Sevick, E. M.; Monson, P. A.; Ottino, J. M. Monte Carlo calculations of cluster statistics in continuum models of composite morphology. *J. Chem. Phys.* **1988**, *88*, 1198−1206.

(50) Ziff, R. M.; McGrady, E. D.; Meakin, P. On the validity of Smoluchowski's equation for cluster−cluster aggregation kinetics. *J. Chem. Phys.* **1985**, *82*, 5269−5274.

(51) Israelachvili, J. N.; Mitchell, D. J.; Ninham, B. W. Theory of Self-Assembly of hydrocarbon amphiphiles into Micelles and Bilayers. *J. Chem. Soc., Faraday Trans.* **1976**, *72*, 1525−1568.

(52) Peri, J. B. The State of Solution of Aerosol OT in Nonaqueous Solvents. *J. Colloid Interface Sci.* **1969**, *29*, 6−15.

(53) Fendler, E. J.; Fendler, J. H.; Medary, R. T.; Seoud, O. A. E. Proton Magnetic Resonance Investigations of Alkylammonium Carboxylate Micelles in Nonaqueous Solvents, II. Effect of Carboxylate structure in Benzene and in Carbon Tetrachloride. *J. Phys. Chem.* **1973**, *77*, 1432−1436.

Received for review February 3, 2000
Revised manuscript received August 29, 2000
Accepted August 30, 2000

IE000144M